

Optically Modulated Propulsion of Electric-Field-Powered Photoconducting Janus Particles

Matan Zehavi,¹ Daniel Sofer,¹ Touvia Miloh,² Orlin D. Velev³, and Gilad Yossifon^{1,2,*}

¹*Faculty of Mechanical Engineering, Micro- and Nanofluidics Laboratory, Technion–Israel Institute of Technology, Technion City 32000, Israel*

²*School of Mechanical Engineering, Tel Aviv University, Ramat Aviv 69978, Israel*

³*Department of Chemical and Biomolecular Engineering, North Carolina State University, Raleigh, NC 27695, USA*



(Received 15 February 2022; revised 25 June 2022; accepted 20 July 2022; published 22 August 2022)

Herein, we demonstrate the ability to optically tune the mobility of electrically powered Janus particles (JPs) that are half-coated with various zinc oxide (ZnO) semiconducting layers, i.e., polycrystalline, amorphous, and amorphous with a SiO₂ passivation layer. The ZnO semiconductor photoresponse causes an increase in its electrical conductivity with light having wavelengths of sufficient photon energy with respect to the semiconductor band gap. This effect, which we name optically modulated electrokinetic propulsion (OMEP), can be harnessed to increase the contrast in polarizability between the dielectric and semiconducting hemispheres, which, in turn, results in an increased electrokinetic mobility. Optical control of electrical field propulsion enables an additional degree of control of JP mobility. We also demonstrate optical modulation of collective behavior and particle-particle interactions for dense semiconducting Janus particle populations.

DOI: 10.1103/PhysRevApplied.18.024060

I. INTRODUCTION

Active particles have emerged as a topic of scientific interest due to their ability to convert energy from their environment into autonomous translational and/or rotational motion (“self-propulsion”) [1–3]. The underlying mechanism driving such motion is encoded in the active particle design, as they asymmetrically draw and dissipate energy, thus creating local field gradients, resulting in particle mobility [4]. For inactive particles, gradients of externally imposed macroscopic fields can lead to particle motion by effects such as electrophoresis [5], dielectrophoresis [6], magnetophoresis [7], and thermophoresis [8,9]. However, these all result in distinct phoretic motion, i.e., migrating en masse in an externally prescribed direction along the applied-field gradients, in clear contrast to self-propelling particles, where each particle is free to travel along its individual trajectory. Active particles are a subject of great research activity and focus, due to their promise in diverse applications, such as remote microsurgery, medical analytics, self-repairing systems, and self-motile devices [10,11].

Electric fields are a facile and controllable source of energy for powering the motion of active particles, as these fields can be modulated in both frequency and intensity. This enables the precise tuning of the induced propulsion

forces exerted on particles in real time (affecting particle motion) and can also simultaneously provide a means for controlling particle-particle interactions [12]. Changes in the frequency of the applied electric fields can switch between several distinct electrokinetic propulsion mechanisms, such as electrohydrodynamic flows [13], induced-charge electrophoresis (ICEP) [14], self-dielectrophoresis (SDEP) [15], and self-electrophoresis by diode rectification [16–18]. By rationally designing particles that respond to ambient ac electric fields using these mechanisms at different frequencies, it is thus possible to make them change multimodally their direction of motion on demand [19].

To supplement the electrical control parameters of frequency and amplitude, we introduce here an additional means of motility control. This is achieved by using Janus microspheres that are half-coated with a semiconductor shell and illuminated by light of varying intensities and wavelengths. Semiconducting materials are photoconductive, meaning that their electronic conductivity is generally increased upon absorption of photons with sufficient photon energy. In the context of electrokinetic propulsion, the photoconductive effect allows us to change and control the amount of free charge carriers within the semiconducting layer, thereby increasing its electrical conductivity and ideally altering its electrical response from that of being dielectric to a conductor. The change in electrical polarizability under an externally applied electric

*yossifon@tx.technion.ac.il; gilad.yossifon@gmail.com

field results in a change of particle mobility through the abovementioned electrokinetic propulsion mechanisms, a phenomenon we term optically modulated electrokinetic propulsion (OMEP). Previous studies involving optical control of photosensitive semiconducting materials under an external electric field report electrorotation of silicon nanowires [20,21]. Studies have also been conducted where particle collective behavior can affect their optical response [22]. The optical activation of active particles reported here adds another degree of control that can be used for addressing only a subpopulation of active particles within a larger heterogeneous population.

II. MATERIALS AND METHODS

The fabrication of semiconducting Janus particles is based on the modification of silica microspheres of $5\text{ }\mu\text{m}$ in diameter (Polysciences Inc., Cat. No. 24332) that are deposited over a standard microscope slide. Following 1-min O_2 plasma cleaning, the metal or semiconductor coating on their top half is deposited. ZnO coatings are 100 nm thick sputter-deposited from a 99.95% pure ZnO target, with a chamber pressure of 3 mTorr and 100-W gun power. Polycrystalline ZnO is deposited at $T = 300\text{ }^\circ\text{C}$ on a rotating stage, while amorphous ZnO is deposited at room temperature in a direct vertical deposition. On some of the amorphous samples, an additional 10-nm-thick layer of SiO_2 is deposited (room-temperature deposition, 200-W gun power, chamber pressure of 3 mTorr). For the metallic coating, 10 nm of Ti and 35 nm of Au are deposited using an *e*-beam evaporator. Following partial coating deposition, the resulting Janus particles are released and suspended for at least 2 h in a low-concentration KCl solution, $3\text{ }\mu\text{S}/\text{cm}$, $\text{pH} = 6.4$, containing 0.05% Vol./Vol. Tween 20 surfactant to reduce particle adhesion to the floor of the test chamber [23].

The test chamber is comprised of two glass slides separated by 360- μm -thick adhesive tape. The bottom side is a 1.1-mm-thick microscope slide covered by a $4\text{--}10\text{ }\Omega/\text{sq}$ ITO layer (Delta technologies, Cat. No. CB-40IN-0111) with a 15-nm sputtered SiO_2 layer on top for suppression of particle adsorption. The top side is a 0.7-mm-thick microscope slide covered by a $4\text{--}10\text{ }\Omega/\text{sq}$ ITO layer (Delta technologies, Cat. No. CB-40IN-1107) with drilled holes of 1 mm in diameter for the inlet and outlet (see Fig. S1 within the Supplemental Material [24]). Copper conductive tapes are used to connect the ITO-coated glass slides to the function generator. The test chamber is placed onto a Nikon TI inverted microscope with an ANDOR iXon3 CMOS camera and a Yokogawa CSU-X1 spinning-disk confocal system. The image light is introduced using the microscope's bright-field light source filtered through a green interference filter. The UV light source is a Prizmatix Mic-LED-365L light-emitting diode (LED), with peak wavelengths of 365 nm, introduced into the light

path through a 400-nm dichroic mirror. The electric field is introduced using an Agilent 33250A function waveform generator amplified with a Falco systems WMA300 amplifier and filtered through a $10\text{-}\mu\text{F}$ capacitor. The signal parameters are monitored for fidelity using a Tektronix TPS 2024 oscilloscope (see Fig. S2 within the Supplemental Material [24]). For light-power-density measurements, the sample is replaced with a photodiode (Ophir photonics PD300 UV sensor) through a 150- μm -diameter circular aperture, measured with an Ophir photonics VEGA power meter. Light-power measurements for the mobility experiments are performed through the same ITO-coated slide used in the test chamber (Delta technologies, Cat. No. CB-40IN-1107).

To directly measure the ZnO -layer conductivity response to light, a photoresistor test structure is fabricated using common photolithography techniques (see Fig. S3 within the Supplemental Material for manufacturing schematics [24]). The photoconductive layer is deposited onto a 1-mm-thick glass slide and patterned into a $0.5 \times 0.5\text{ mm}^2$ photoresistor, in the same deposition process as the Janus particles. Electrical contacts of 50-nm-thick Ti followed by 200-nm-thick Au are deposited by an ion-beam evaporator and soldered to wires for connectivity.

III. RESULTS

A. OMEP

The electrokinetic mobility of a Janus particle (JP) relies on the contrast between the electrical polarizabilities of its opposite hemispheres. The electrical conductivity of the ZnO -coated JP side is changed due to illumination by light of wavelengths that have sufficient photon energy relative to the coating band gap. The active particle mobility can be thus controlled by means of ICEP [Fig. 1(a)] and SDEP electrokinetic propulsion mechanisms. We coat the Janus particles with polycrystalline ZnO [Fig. 1(b)], a semiconductor material with a band gap of about 3.4 eV [25], to achieve a response to light activation with wavelengths below 365 nm. Figure 1(c) shows a particle's velocity response to UV under a fixed electric field amplitude and frequency, when suspended in low-conductivity ($3\text{ }\mu\text{S}/\text{cm}$) KCl solution. As clearly seen, the particle velocity increases significantly with UV illumination. The small velocity without UV light is a result of the non-negligible polycrystalline ZnO dark conductivity [see Fig. 2(c)]. No mobility response is observed when applying UV light with no external electric field (see Video S1 within the Supplemental Material [24]). Therefore, self-thermophoretic [26,27] and photocatalytic [28] mechanisms can be excluded as a cause for particle propulsion. Thermal convection effects can also be negated due to our test conditions of low-conductivity solution ($3\text{ }\mu\text{S}/\text{cm}$) and spatially uniform applied electric field (supported also

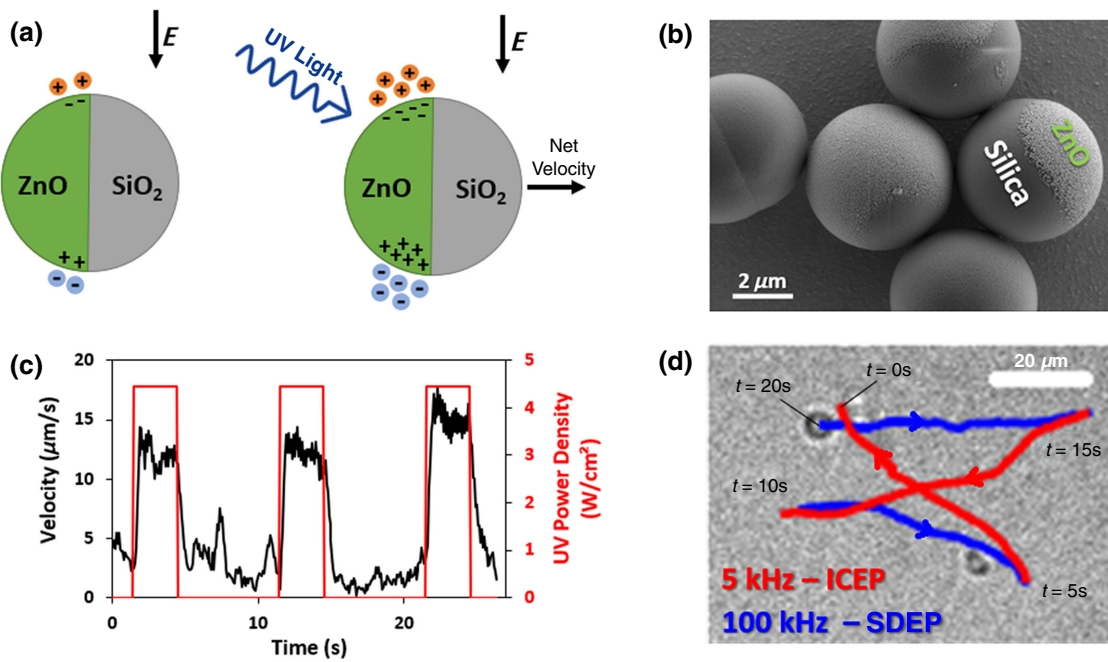


FIG. 1. Optically modulated electrokinetic propulsion (OMEPP). (a) Schematics of the optical (UV) gated mobility of electrically powered semiconducting Janus particles at low frequencies corresponding to ICEP mode. (b) SEM image of silica microparticles half-coated with a 100-nm-thick layer of polycrystalline ZnO. (c) Representative velocity plot of a Janus particle at 8 kHz, 166.7 kVpp/m, electric field under UV (365 nm) light switching. (d) JP trajectory under continuous illumination of UV light with electric field frequency switching between 5 and 100 kHz, corresponding to ICEO and SDEP propulsion modes, respectively, acting in opposite directions. See Video S1 within the Supplemental Material [24] for representative mobility videos.

by the scaling analysis of Zehavi *et al.* [29]). To illustrate the transition between different electrokinetic propulsion modes, Fig. 1(d) shows a Janus-particle path traced under frequency switching between 5 and 100 kHz subject to fixed UV illumination and electric field amplitude. The propulsion mechanisms that are switched correspond to ICEO and SDEP and act in opposite directions.

B. Photoconductivity characterization

The ZnO test structure Fig. 2(a) is exposed to different intensities of UV light and its electrical behavior is evaluated using *I-V* measurements, using a Keithley 2636A source meter (see Fig. S4 within the Supplemental Material [24]). To examine the wavelength dependency (quantum effect) of the photoconductive response, we illuminate the photoresistor with varying wavelengths at the same power density and measure its conductivity [Fig. 2(b)]. It can be clearly seen that, for wavelengths higher than 365 nm, which correspond to the ZnO band-gap energy, the photoconductivity decreases by a few orders of magnitude, as expected from ZnO absorption [30]. However, for wavelengths near the band gap, the photoconductivity response is found to be sufficient for the JP to clearly exhibit propulsion (see Fig. S5 within the Supplemental Material for

the mobility response of a polycrystalline ZnO JP under illumination at 390 nm [24]).

As seen in Fig. 2(c), the electronic conductivity of the semiconductor layer can be continuously tuned via variation of the power density of UV illumination. We further demonstrate the ability to tune the mobility of a Janus particle via optical gating of varying optical power densities under a continuous fixed electric field [Fig. 2(d) and Video S1 within the Supplemental Material [24]].

C. Characterization of photoconductive JP mobility

Figure 3(a) depicts the frequency dispersion of JP mobility under a constant applied ac electric field of 166.7 kVpp/m and UV-activation power density of 4.4 W/cm². The photoconductive particles show a similar frequency-response behavior to that of the controlled metallo dielectric (“Au”) particles, demonstrating distinct low-frequency ICEP and high-frequency SDEP regions. In accordance with the photoconductive responses measured for the different coating types, the mobility of the ZnO Janus particles changes with the coating conductivity. Data in Fig. 3(b) show increasing JP mobility by optically changing the semiconductor conductivity. These experimental results are in qualitative agreement with the theoretical predictions in Ref. [31] for ICEP. The results for the

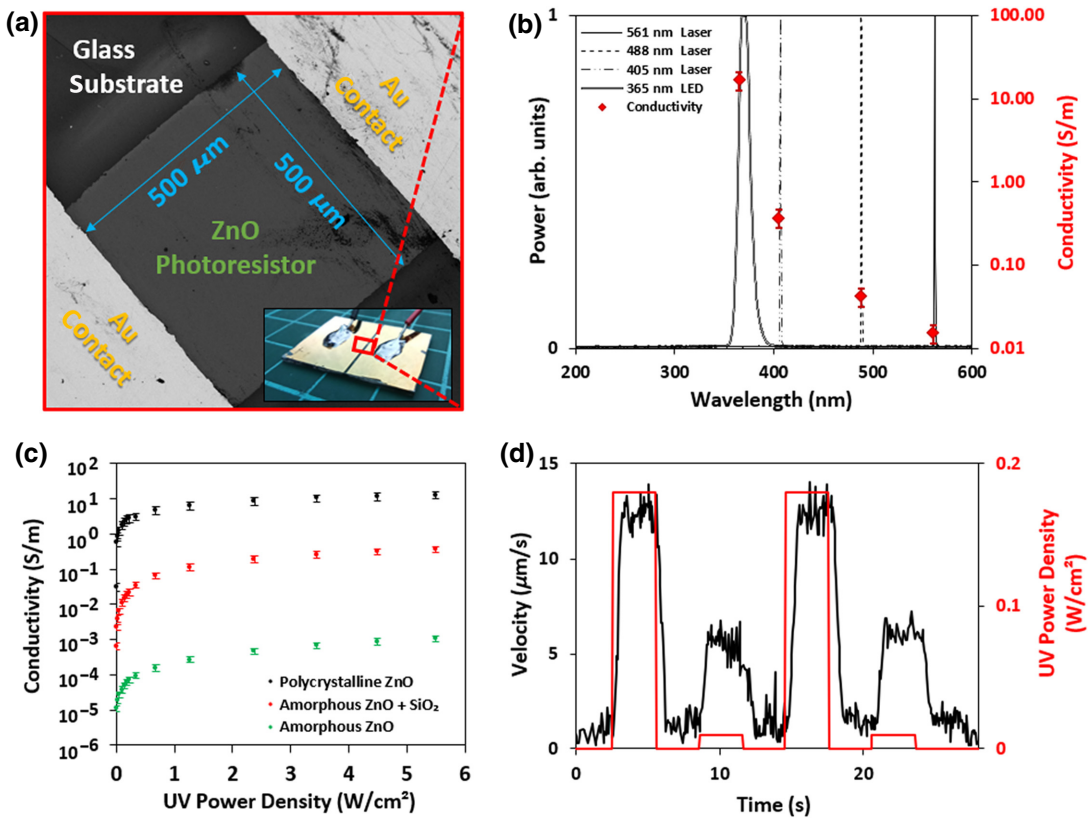


FIG. 2. Optical control over electrical conductivity and Janus particle mobility. (a) SEM image of the conductivity test structure used in the photoconductivity measurements; inset, photograph of a test chip. (b) Conductivity measurements of polycrystalline ZnO test structure under various illumination sources at 0.14 W/cm^2 and their source spectrum. (c) Electrical conductivity measurements of different types of ZnO photoresponsive coatings under varying UV (365 nm) illumination intensity. Measurement corresponding to zero UV power density is taken under ambient light conditions. (d) Effect of dynamic optical gating of polycrystalline ZnO JP mobility at varying optical power densities, under constant application of an electric field of 100 kHz and 166.7 kVpp/m . Error bars in (b),(c) represent the standard deviation of ZnO-layer thickness that is inversely related to the measured conductance.

SDEP region are in qualitative agreement with the numerically calculated JP velocity [see inset of Fig. 3(b)], exhibiting a monotonic increase in magnitude with increasing electrical conductivity, σ_i , of the semiconducting coating. Boundary-condition formulation and simulation details are available in Appendixes A and B.

D. Collective response in a densely populated photoconductive JP system

The collective behavior of a high-density population of amorphous ZnO JPs with SiO_2 passivation, as well as polycrystalline ZnO JPs and bare silica beads, is explored by applying a fixed-amplitude electric field at low (8 kHz) and high (1 MHz) frequencies while transitioning between UV *on* and *off* states. The images in Fig. 4 depict the behavior of the three different particle types, as well as their motion path, along within a 5-s period to give a qualitative sense of their mobility and collective behavior. To avoid the transients upon application of an electric field with UV *off*,

analysis begins 5 s after the application of the field. In the low-frequency regime and upon electric field activation with UV *off*, the JPs behave as dielectric silica spheres and self-assemble into a structure with uniform interparticle spacing. Upon UV illumination, the JPs still exhibit repulsive dipolar interactions with neighboring particles [due to the induced electric double layer (EDL) screening of the photoactivated semiconducting hemisphere], while some of the JPs move due to ICEP effects.

At the other extreme end of the high-frequency region, as demonstrated in the 1 MHz case, there is practically no induced EDL screening of the JPs. Therefore, the JP can be considered as an entity including two dipoles of opposite directions, corresponding to the dielectric and semiconducting sides. With no UV activation, the amorphous ZnO with SiO_2 passivation JP's collective response is similar to that of the 8-kHz case as the semiconducting hemisphere is not photoactivated, and the dielectric dipole dominates dipolar repulsion. However, under UV exposure, we observe an attractive dipolar

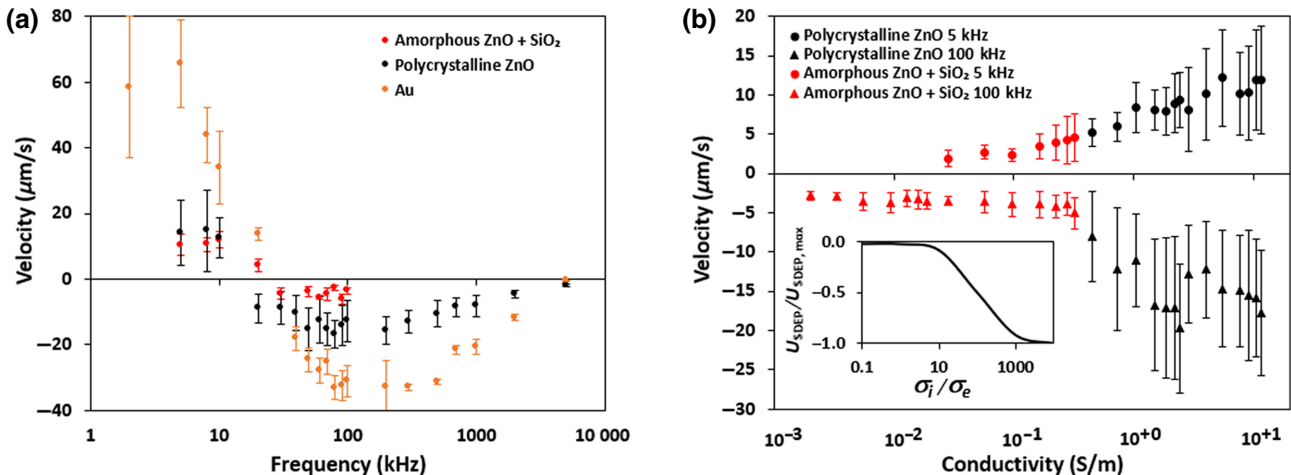


FIG. 3. Frequency dispersion of the JP mobility and its dependency on the optical illumination intensity. (a) Mobility of JPs with different coatings versus frequency under an applied electric field of 166.7 kVpp/m and 4.4 W/cm² UV intensity (365 nm). (b) Dependency of JP mobility on ZnO conductivity (subject to UV intensity; see Fig. S6 within the Supplemental Material [24]) at applied electric field frequencies of 5 and 100 kHz under 166.7 kVpp/m and corresponding to ICEP and SDEP modes, respectively. The transition from UV intensity to electrical conductivity was based on the experimental measurements depicted in Fig. 2(c). Inset: Numerically calculated normalized JP velocity (under SDEP mode at a normalized frequency of $\tilde{\Omega} = (\omega\lambda_0 a/D) = 100$) for varying ratio of semiconducting coating (σ_i) to electrolyte solution (σ_e) conductivities. Error-bars are velocity standard deviation.

interaction between the dipole of the dielectric JP side with the corresponding dipole of its neighbor's photoactivated semiconducting side, resulting in chain formation. These results are in qualitative agreement with previous findings [32–34], which also observe such collective behavior but with metallic (Au) coated JPs at the low- and high-frequency extremes. They suggested that the dielectric dependent frequency mismatch between the two JP hemispheres allowed simultaneous control of particle mobility and colloidal interactions. For a similar ITO parallel-plate system, [32] it is shown that it is possible to reconfigure active particles into various collective states by

introducing imbalanced interactions to realize phases of swarms, chains, clusters, and isotropic gases from the same precursor particle by changing the electric field frequency.

To further understand the effect of optical modulation on the JP's collective behavior, we generalize the JP-JP dipolar interaction model of Yan *et al.* [32] to account for the electric field frequency and complex permittivity of the semiconducting hemisphere with varying electrical conductivity. The model is in qualitative agreement with the experiments, in the sense that it succeeds at predicting the repulsive interaction at low frequencies (regardless

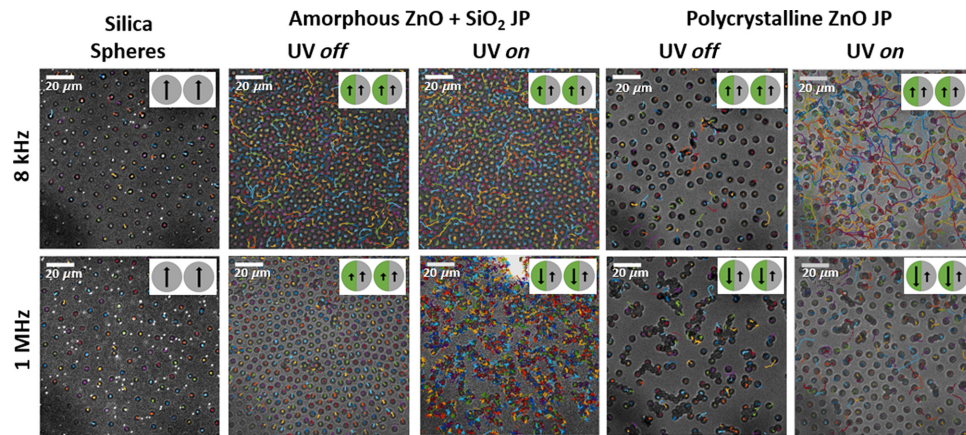


FIG. 4. Collective behavior of highly dense JPs of different types shown for 8 kHz and 1 MHz frequencies under 166.7 kVpp/m electric field, with and without UV activation (7 W/cm²). Path trajectories are drawn for a period of 5 s. The corresponding MSD (mean square displacement) analysis is depicted in Fig. S7 within the Supplemental Material [24]. See also Videos S2 and S3 within the Supplemental Material [24].

of UV illumination), as well as the transition to attractive interactions (i.e., formation of chains) with increasing frequency and UV illumination (see Appendix C for details).

IV. CONCLUSIONS AND OUTLOOK

To summarize, we report an approach for controlling the mobility of electrokinetically driven active Janus particles and modulating their collective behavior by means of optically controlling the electrical properties of their semiconducting half-sphere coating. Specifically, we use silica particles that are half-coated with photoconductive ZnO layers to form a Janus particle with a semiconducting side. We characterize the photoconductivity effect using a test chip for several coating types (polycrystalline ZnO, amorphous ZnO, and amorphous ZnO with a passivation SiO₂ layer) for varying optical illumination intensities and wavelengths. We then proceed to measure the velocity of electrokinetically driven JPs under varying electric fields and UV power densities. The results show that the added degree of UV-light control enables not just “on-off” switching but also continuous tuning of the electrokinetic ICEP and sDEP velocities for isolated particles. The optically modulated electrokinetic propulsion also allows efficient control and switching between different collective behavior types in dense particle populations, by tuning the JP-induced dipoles and the resulting dipolar interaction between interacting JPs. This control of OMEP enables additional degrees of freedom in active semiconducting particle design, as they can be selectively activated within a heterogenous population of particles by judicious selection of the excitation wavelength (i.e., according to the band gap of different semiconducting coatings). Combining different semiconducting coatings onto the same active particle can also enable control of not only its velocity but also its trajectory via deterministic optical steering (unlike purely electrical steering [35], in which random diffusional rotation is harnessed into directed motion using a feedback-based particle-guiding method), as well as the collective interactions of systems of such engineered active particles.

ACKNOWLEDGMENTS

M.Z., G.Y., T.M., and O.V. wish to acknowledge support from the Binational Science Foundation (BSF) Grant No. 2018168. O.V. also acknowledges partial support from NSF Grant No. CBET-2133983. We wish to acknowledge the Technion Russel-Berrie Nanotechnology Institute (RBNI) and the Technion Micro-Nano Fabrication Unit (MNFU) for their technical support. We thank Professor Yosi Shacham-Diamand from Tel-Aviv University for his valuable advice and inputs regarding the photoconductive effects and processes.

APPENDIX A: ANALYTICAL FORMULATION OF AN EFFECTIVE BOUNDARY CONDITION FOR A MACROSCALE (i.e., OUTSIDE THE EDL) SOLUTION FOR JANUS PARTICLES WITH VARYING COMPLEX PERMITTIVITY

In the case of a polarizable particle placed in a uniform ac field, utilizing the standard model based on the linearized (weak-field) formulation [36], one can obtain an expression for the relationship between the phasors of the electric potential, ϕ_e (normalized with respect to the thermal scale, $\varphi_1 = k_B T/ze$), and the charge density, Q_e (normalized by zen_∞ , where n_∞ is the number of ions in the bulk under equilibrium), in terms of the physical (real) Debye length, λ_o , as

$$\lambda^2 \nabla^2 Q_e = Q_e = -2\lambda_0^2 \nabla^2 \phi_e, \quad \frac{1}{\lambda^2} = \frac{1}{\lambda_0^2} + \frac{i\omega}{D}. \quad (\text{A1})$$

Thus, the corresponding expressions for the electric potential and charge distribution are given by $\text{Re}[(\phi_e, Q_e)e^{i\omega t}]$, where $\text{Re}[]$ represents the real part; ω is the forcing frequency and D denotes the diffusivity of the (symmetric) electrolyte. The solution to Eq. (A1) can be written as

$$2\phi_e = -\left(\frac{\lambda}{\lambda_0}\right)^2 Q_e + \chi_e, \quad \nabla^2 \chi_e = 0, \quad (\text{A2})$$

where χ_e is a harmonic function to be determined. The fact that the particle surface is impervious to both ions and cations renders [36]

$$2\frac{\partial \phi_e}{\partial R} + \frac{\partial Q_e}{\partial R} = \left(1 - \left(\frac{\lambda}{\lambda_0}\right)^2\right) \frac{\partial Q_e}{\partial R} + \frac{\partial \chi_e}{\partial R} = 0, \quad (\text{A3})$$

wherein R is the radial coordinate normalized by the particle radius, a . For a thin EDL ($\lambda_0/a \ll 1$), it is plausible to assume that $(\partial Q_e/\partial R) \sim -(aQ_e/\lambda)$. Denoting the phasor of the interior (inside the particle) potential as ϕ_i and the corresponding complex permittivities in a fluid and particle as $\tilde{\epsilon}_{e,i} = \epsilon_{e,i} + (i\sigma_{e,i}/\omega)$, the boundary conditions on the surface of the particle, S , can be expressed as

$$\phi_e = \phi_i, \quad (\text{A4})$$

$$\tilde{\epsilon}_e \frac{\partial \phi_e}{\partial R} = \tilde{\epsilon}_i \frac{\partial \phi_i}{\partial R} = -\frac{\tilde{\epsilon}_e}{2} \frac{\partial Q_e}{\partial R} = \frac{\tilde{\epsilon}_e (\partial \chi_e / \partial R)}{2(1 - (\lambda/\lambda_0)^2)}. \quad (\text{A5})$$

Assuming, for simplicity, that ϕ_i depends linearly (to leading order) on R , this implies that $(\partial \phi_i / \partial R) \sim \phi_i$ on $R = 1$,

and thus,

$$\begin{aligned}\frac{\partial \chi_e}{\partial R} &\sim -\frac{a}{\lambda} \left(1 - \left(\frac{\lambda_0}{\lambda}\right)^2\right) \left(\frac{\lambda}{\lambda_0}\right)^2 Q_e \\ &= -\frac{a}{\lambda} \left(1 - \left(\frac{\lambda_0}{\lambda}\right)^2\right) (\chi_e - 2\phi_e),\end{aligned}\quad (\text{A6})$$

or

$$\begin{aligned}\frac{\partial \chi_e}{\partial R} &= -\frac{a}{\lambda} \left(1 - \left(\frac{\lambda_0}{\lambda}\right)^2\right) \left(\chi_e - 2\frac{\partial \phi_i}{\partial R}\right) \\ &= -\frac{a}{\lambda} \left(1 - \left(\frac{\lambda_0}{\lambda}\right)^2\right) \left(\chi_e - \frac{(\tilde{\epsilon}_e/\tilde{\epsilon}_i)(\partial \chi_e/\partial R)}{(1 - (\lambda/\lambda_0)^2)}\right),\end{aligned}\quad (\text{A7})$$

from which one obtains

$$\begin{aligned}\frac{\partial \chi_e}{\partial R} &= \frac{-(a/\lambda)(1 - (\lambda_0/\lambda)^2)}{1 + (a/\lambda)(\lambda_0/\lambda)^2(\tilde{\epsilon}_e/\tilde{\epsilon}_i)} \chi_e \\ &= \frac{i \tilde{\Omega}(\lambda_0/\lambda)}{1 + (a/\lambda)(\lambda_0/\lambda)^2(\tilde{\epsilon}_e/\tilde{\epsilon}_i)} \chi_e,\end{aligned}\quad (\text{A8})$$

wherein $\tilde{\Omega} = \omega \lambda_0 a / D$ represents the dimensionless frequency scaled by the corresponding RC frequency.

APPENDIX B: NUMERICAL SIMULATIONS

A simplified two-dimensional numerical simulation of the electrostatic problem is performed in COMSOL™ 5.3 following the procedure used by Boymelgreen *et al.* [37]. Herein, we focus only on solving the SDEP response of the JP particle, which extends the previously obtained solution for the ICEP response [31]. The height of the domain is set at $H = 10a$, where a is the radius of the Janus particle. The particle is positioned at a distance $h = 0.01a$ (measured from the bottom of the particle) above a powered electrode. This value of the gap between the JP and the bottom substrate is chosen somewhat arbitrarily, as we cannot experimentally measure it for a moving JP. In our recent paper [37], we performed a parameteric study of varying gap values and found the resulting JP velocity to be highly sensitive to it.

The electrodes are subject to a voltage difference directed along the x_2 direction with a magnitude of $V(t) = \text{Re}\{V_0 e^{i\omega t}\}$, where V_0 is the peak magnitude. Recognizing that, for micron-sized particles, the physical Debye length, λ_0 , is much smaller than the particle radius ($\lambda_0/a \ll 1$). The distributed charge, Q_e , is located in a thin layer adjacent to the solid-liquid interfaces such that, outside this layer, $Q_e \rightarrow 0$, and one can thus describe the electric field in the bulk by Laplace's equation, $\nabla^2 \chi_e = 0$. The bottom electrode is polarizable and subject to an

applied field of magnitude 1 V, while the upper electrode is grounded ($V = 0$). The electrostatic boundary condition for the lower electrode is of a mixed (Robin) type and can be written in terms of the normal derivative as $(\partial \chi_e/\partial R)|_{x_2=0} = i\tilde{\Omega}(\chi_e - 1)$, where lengths are scaled by a . The boundary condition on the right metallic hemisphere of the JP is described by simplifying Eq. (A8) using the assumption that the applied frequency is much smaller than the Maxwell-Wagner relaxation time of the EDL, $\Omega = (\omega \lambda_0^2/D) = \tilde{\Omega}(\lambda_0/a) \ll 1$, yielding $(\partial \chi_e/\partial R) = (i\tilde{\Omega}(\chi_e - \chi_0)/(1 + (a/\lambda_0)(\tilde{\epsilon}_e/\tilde{\epsilon}_i)))$. Herein, χ_0 represents a reference potential to obey the zero-induced net charge condition on the particle. The dielectric (left side) of the JP is assumed to be insulating, satisfying a Neumann-type boundary condition of $(\partial \chi_e/\partial R) = 0$. The electrostatic force is then obtained by the integration of the time-averaged Maxwell stress tensor, M_{ij} , over the surface of the Janus sphere, namely, $F_E^{(i)} = \int_S M_{ij} n_j dS$; $M_{ij} = (1/2)\text{Re}\{(\partial \chi_e/\partial x_i)(\partial \chi_e^*/\partial x_j) - (1/2)(\partial \chi_e/\partial x_k)(\partial \chi_e^*/\partial x_k)\delta_{ij}\}$, where $*$ denotes the complex conjugate and S is any surface that envelopes the particle. The corresponding velocity for a freely suspended particle is finally found by equating the nondimensional electrostatic force applied in the x_1 direction to the corresponding dimensionless Stokes drag, $F_{\text{drag}} = 6\pi U f$, where f denotes the correction factor of Stokes' law due to wall proximity [37]. However, since we seek here only qualitative behavior, we normalize the electrostatic force by its maximum value in the inset of Fig. 3(b).

APPENDIX C: A MODEL FOR JP-JP INTERACTIONS

Herein, we generalize the JP-JP interaction model of Yan *et al.* [32] to account for the electric field frequency and complex permittivity of the semiconducting hemisphere. Consider an isotropic spherical particle of radius a and complex permittivity $\tilde{\epsilon}_p = \epsilon_p + (i(\sigma_p + \sigma_\Sigma))/\omega$ suspended within a symmetric unbounded electrolyte, $\tilde{\epsilon}_e = \epsilon_e + (i\sigma_e/\omega)$, and subjected to a uniform electric field, $E_0 e^{i\omega t}$, wherein $\sigma_\Sigma = (2/a)K_s$ is the effective conductivity stemming from the surface conductance, K_s . Based on our previous work [37], the equivalent dipole, normalized by $4\pi \epsilon_e a^3 E_0$, is given by

$$d = -\frac{1}{2} + \frac{(3/2)i\Omega}{2(\lambda/\lambda_0)^2(1 + (a/\lambda)(\tilde{\epsilon}_e/\tilde{\epsilon}_p)) + i\Omega(1 + 2(\tilde{\epsilon}_e/\tilde{\epsilon}_p))}, \quad (\text{C1})$$

where $\Omega = (\omega \lambda a / D)$, $(1/\lambda^2) = (1/\lambda_0^2) + (i\omega/D)$. For a low frequency, $(\lambda/\lambda_0)^2 = 1$, and metallic sphere, $(\tilde{\epsilon}_e/\tilde{\epsilon}_p) \ll (\lambda/a)$, we get $d_{\text{low}} = -(1/2) + ((3/2)i\Omega)/$

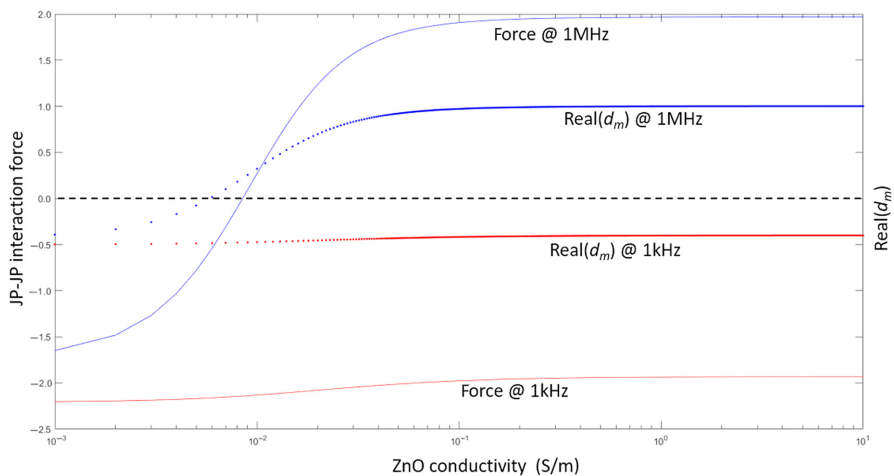


FIG. 5. Calculated interaction force between JP-JP particles for varying ZnO conductivity and low (1 kHz) and high (1 MHz) frequency levels.

$(2 + i\Omega)$, which, for a dc ($\Omega = 0$), gives $d_{dc} = -1/2$. For high frequencies, $(\lambda/\lambda_0)^2 \rightarrow 0$ and $d_{high} = -(1/2) + (3/2)/(1 + 2(\tilde{\epsilon}_e/\tilde{\epsilon}_p)) = ((1 - (\tilde{\epsilon}_e/\tilde{\epsilon}_p))/(1 + 2(\tilde{\epsilon}_e/\tilde{\epsilon}_p)))$. Thus, the general dipole term provides a unified dispersion for all frequencies (including low-frequency EDL screening and the Clasius-Mossotti term for high frequency).

Next, consider the JP pair model of Yan *et al.* [32] for metalodielectric hemispheres, denoting the corresponding dipoles as d_m (metallic/semiconducting) and d_d (dielectric). Since both dipoles are complex, the dimensional electrostatic attractive force between the two JPs can be written, in terms of dimensional dipoles, as

$$F = -\frac{3}{8\pi\epsilon_0} \frac{1}{(2a)^4} \left[d_m d_m^* + d_d d_d^* + \frac{1}{2} (d_d d_m^* + d_m d_d^*) \left(\left(\frac{8}{11}\right)^4 + \left(\frac{8}{5}\right)^4 \right) \right]. \quad (C2)$$

Assuming a perfect dielectric, $(\tilde{\epsilon}_e/\tilde{\epsilon}_p) \gg 1$, one gets $\text{Re}(d_d) \sim -(1/2)$ and $\text{Im}(d_d) \sim 0$.

Figure (5) depicts the JP-JP interaction force, Eq. (C2) (only the expression in the square brackets with the minus sign), calculated for a JP of radius $a = 5 \mu\text{m}$, silica dielectric constant $\epsilon_d/\epsilon_0 = 3.5$, ZnO dielectric constant $\epsilon_m/\epsilon_0 = 8.5$, silica effective conductivity $\sigma_d = 1 \times 10^{-4} \text{ S/m}$ [38], ionic diffusion coefficient $D = 2 \times 10^{-9} \text{ m}^2/\text{s}$, electrolyte conductivity $\sigma_e = 3 \times 10^{-4} \text{ S/m}$, and electrolyte dielectric constant $\epsilon_e/\epsilon_0 = 80$, wherein $\epsilon_0 = 8.854 \times 10^{-12} \text{ F/m}$ is the vacuum permittivity. Interestingly, it explains the JP-JP repulsion at low frequency (8 kHz) (negative value) seen in Fig. 4 for all particle types with or without UV. In the high-frequency regime (1 MHz), it also explains the transition from repulsive to attractive JP-JP interactions observed for the case of amorphous ZnO with

SiO_2 coating upon UV illumination. In this case, the force changes its sign upon photoactivation (conductivity increase to $\sim 10^{-2} \text{ S/m}$), which is in qualitative accordance with measured photoconductivity values. Furthermore, the dark conductivity of polycrystalline ZnO [see Fig. 2(c)] is of the same order as the abovementioned case, explaining the JP-JP chains formation observed even without UV illumination (see Fig. 4).

-
- [1] C. W. Shields and O. D. Velev, The evolution of active particles: Toward externally powered self-propelling and self-reconfiguring particle systems, *Chem* **3**, 539 (2017).
 - [2] J. Zhang, E. Luijten, B. A. Grzybowski, and S. Granick, Active colloids with collective mobility status and research opportunities, *Chem. Soc. Rev.* **46**, 5551 (2017).
 - [3] C. Hu, S. Pane, and B. J. Nelson, Soft micro- and nanorobotics, *Annu. Rev. Control Robot. Auton. Syst.* **1**, 53 (2018).
 - [4] K. Han, C. Wyatt, O. D. Velev, K. Han, C. W. Shields, and I. O. D. Velev, Engineering of self-propelling microbots and microdevices powered by magnetic and electric fields, *Adv. Funct. Mater.* **28**, 1705953 (2018).
 - [5] J. M. Karlinsey, Sample introduction techniques for microchip electrophoresis: A review, *Anal. Chim. Acta* **725**, 1 (2012).
 - [6] R. Pethig, Review article—dielectrophoresis: Status of the theory, technology, and applications, *Biomicrofluidics* **4**, 022811 (2010).
 - [7] N. Pamme and A. Manz, On-chip free-flow magnetophoresis: Continuous flow separation of magnetic particles and agglomerates, *Anal. Chem.* **76**, 7250 (2004).
 - [8] F. Zheng, Thermophoresis of spherical and non-spherical particles: A review of theories and experiments, *Adv. Colloid Interface Sci.* **29**, 255 (2002).
 - [9] F. M. Weinert and D. Braun, Observation of Slip Flow in Thermophoresis, *Phys. Rev. Lett.* **101**, 168301 (2008).

- [10] J. Li, O. E. Shklyaev, T. Li, W. Liu, H. Shum, I. Rozen, A. C. Balazs, and J. Wang, Self-propelled nanomotors autonomously seek and repair cracks, *Nano Lett.* **15**, 7077 (2015).
- [11] Y. Wu, A. Fu, and G. Yossifon, Active particles as mobile microelectrodes for selective bacteria electroporation and transport, *Sci. Adv.* **6**, eaay4412 (2020).
- [12] O. D. Velev and K. H. Bhatt, On-chip micromanipulation and assembly of colloidal particles by electric fields, *Soft Matter* **2**, 738 (2006).
- [13] F. Ma, X. Yang, H. Zhao, and N. Wu, Inducing Propulsion of Colloidal Dimers by Breaking the Symmetry in Electrohydrodynamic Flow, *Phys. Rev. Lett.* **115**, 208302 (2015).
- [14] S. Gangwal, O. J. Cayre, M. Z. Bazant, and O. D. Velev, Induced-Charge Electrophoresis of Metallodielectric Particles, *Phys. Rev. Lett.* **100**, 058302 (2008).
- [15] A. Boymelgreen, G. Yossifon, and T. Miloh, Propulsion of active colloids by self-induced field gradients, *Langmuir* **32**, 9540 (2016).
- [16] S. T. Chang, V. N. Paunov, D. N. Petsev, and O. D. Velev, Remotely powered self-propelling particles and micropumps based on miniature diodes, *Nat. Mater.* **6**, 235 (2007).
- [17] R. Sharma, O. D. Velev, R. Sharma, and O. D. Velev, Remote steering of self-propelling microcircuits by modulated electric field, *Adv. Funct. Mater.* **25**, 5512 (2015).
- [18] U. Ohiri, C. W. Shields, K. Han, T. Tyler, O. D. Velev, and N. Jokerst, Reconfigurable engineered motile semiconductor microparticles, *Nat. Commun.* **9**, 1791 (2018).
- [19] C. W. Shields, K. Han, F. Ma, T. Miloh, G. Yossifon, and O.D. Velev, Supercolloidal spinners: Complex active particles for electrically powered and switchable rotation, *Adv. Funct. Mater.* **28**, 1803465 (2018).
- [20] Z. Liang and D. Fan, Visible light-gated reconfigurable rotary actuation of electric nanomotors, *Sci. Adv.* **4**, eaau0981 (2018).
- [21] Z. Liang, D. Teal, and D. Fan, Light programmable micro/nanomotors with optically tunable in-phase electric polarization, *Nat. Commun.* **10**, 5275 (2019).
- [22] H. Gao, Y. Xu, K. Yao, and Y. Liu, Self-assembly of silica-gold core-shell microparticles by electric fields toward dynamically tunable metamaterials, *ACS Appl. Mater. Interfaces* **13**, 14417 (2021).
- [23] D. Nishiguchi and M. Sano, Mesoscopic turbulence and local order in Janus particles self-propelling under an ac electric field, *Phys. Rev. E: Stat., Nonlinear, Soft Matter Phys.* **92**, 052309 (2015).
- [24] See the Supplemental Material at <http://link.aps.org/supplemental/10.1103/PhysRevApplied.18.024060> for videos and supporting figures.
- [25] D. Vogel, P. Krüger, and J. Pollmann, *Ab initio* electronic-structure calculations for II-VI semiconductors using self-interaction-corrected pseudopotentials, *Phys. Rev. B* **52**, R14316 (1995).
- [26] H. R. Jiang, N. Yoshinaga, and M. Sano, Active Motion of a Janus Particle by Self-Thermophoresis in a Defocused Laser Beam, *Phys. Rev. Lett.* **105**, 268302 (2010).
- [27] E. J. Avital and T. Miloh, Self-thermophoresis of laser-heated spherical Janus particles, *Eur. Phys. J. E* **44**, 139 (2021).
- [28] M. Ni, M. K. H. Leung, D. Y. C. Leung, and K. Sumathy, A review and recent developments in photocatalytic water-splitting using TiO₂ for hydrogen production, *Renewable Sustainable Energy Rev.* **11**, 401 (2007).
- [29] M. Zehavi, A. Boymelgreen, and G. Yossifon, Competition between Induced-Charge Electro-Osmosis and Electrothermal Effects at Low Frequencies Around a Weakly Polarizable Microchannel Corner, *Phys. Rev. Appl.* **5**, 044013 (2016).
- [30] J. F. Muth, R. M. Kolbas, A. K. Sharma, S. Oktyabrsky, and J. Narayan, Excitonic structure and absorption coefficient measurements of ZnO single crystal epitaxial films deposited by pulsed laser deposition, *J. Appl. Phys.* **85**, 7884 (1999).
- [31] A. M. Boymelgreen and T. Miloh, Alternating current induced-charge electrophoresis of leaky dielectric Janus particles, *Phys. Fluids* **24**, 082003 (2012).
- [32] J. Yan, M. Han, J. Zhang, C. Xu, E. Luijten, and S. Granick, Reconfiguring active particles by electrostatic imbalance, *Nat. Mater.* **15**, 1095 (2016).
- [33] S. Gangwal, O. J. Cayre, and O. D. Velev, Dielectrophoretic assembly of metallodielectric Janus particles in ac electric fields, *Langmuir* **24**, 13312 (2008).
- [34] S. Gangwal, A. Pawar, I. Kretzschmar, and O. D. Velev, Programmed assembly of metallodielectric patchy particles in external ac electric fields, *Soft Matter* **6**, 1413 (2010).
- [35] T. Mano, J. B. Delfau, J. Iwasawa, and M. Sano, Optimal run-and-tumble-based transportation of a Janus particle with active steering, *Proc. Natl. Acad. Sci. U. S. A.* **114**, E2580 (2017).
- [36] T. Miloh, A unified theory of dipolophoresis for nanoparticles, *Phys. Fluids* **20**, 107105 (2008).
- [37] A. M. Boymelgreen, G. Kunti, P. Garcia-Sanchez, A. Ramos, G. Yossifon, and T. Miloh, The role of particle-electrode wall interactions in mobility of active Janus particles driven by electric fields, *J. Colloid Interface Sci.* **616**, 465 (2022).
- [38] L. Rozitsky, A. Fine, D. Dado, S. Nussbaum-Ben-Shaul, S. Levenberg, and G. Yossifon, Quantifying continuous-flow dielectrophoretic trapping of cells and micro-particles on micro-electrode array, *Biomed. Microdevices* **15**, 859 (2013).